



Stabilization of Prussian blue using copper sulfate for eliminating radioactive cesium from a high pH solution and seawater

Shoichi Manabe^{a,c,*}, Adavan Kiliyankil Vipin^{a,*}, Tsuguo Kumashiro^c, Shoichi Takiguchi^c, Bunshi Fugetsu^b, Ichiro Sakata^{a,b}

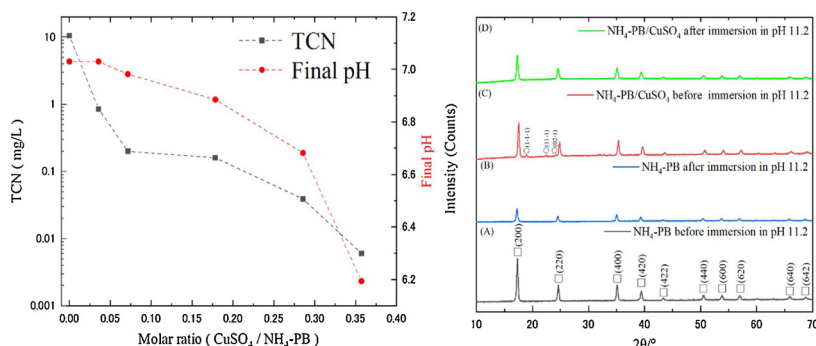
^a School of Engineering, The University of Tokyo, 7-3-1 Bunkyo-Ku, Tokyo 113-8656, Japan

^b Policy Alternatives Research Institute, The University of Tokyo, 7-3-1 Bunkyo-Ku, Tokyo 113-0033, Japan

^c Nanosummit Co. Ltd., Kawaguchi City, Kamiaoki 3-12, Saitama, Japan



GRAPHICAL ABSTRACT



ARTICLE INFO

Editor: Daniel C.W. Tsang

Keywords:

Prussian blue

Copper sulfate

Stabilizer

Cyanide suppression

Cesium adsorption

ABSTRACT

Prussian blue (PB), an adsorbent for the selective elimination of radioactive cesium from water, is highly versatile due to its unique crystal structure. However, PB crystals quickly decompose in an alkaline solution, generating hazardous cyanide contamination. In this research, the alkaline susceptibility of PB was remedied by incorporating copper sulfate as a protector. A stability assessment was conducted at several environmental conditions, such as high pH and temperatures from 10 °C to 50 °C, in seawater, artificial seawater, and river water. The crystalline and chemical stability of PB in the new class of composite was extremely high, even at a pH value of 11.2, as confirmed using XRD and total cyanide analysis. A comprehensive mechanism study revealed that, at high pH, the copper ions that cover the PB react with hydroxide ions to form copper hydroxide and shielding inner crystals. To decontaminate radioactive cesium, the first step was to immobilize nano PB on a cellulose nanofiber, followed by copper sulfate stabilization. Then, a spongiform adsorbent was made using polyurethane as the precursor. The new stabilized PB showed promising adsorption efficiency. Thus, this research will open a new range of applications for all existing and emerging PB-based adsorbents.

* Corresponding authors at: School of Engineering, The University of Tokyo, 7-3-1 Bunkyo-Ku, Tokyo 113-8656, Japan.

E-mail addresses: manabe@ipr-ctr.t.u-tokyo.ac.jp (S. Manabe), vipin@ipr-ctr.t.u-tokyo.ac.jp (V. Adavan Kiliyankil).

1. Introduction

On 2011-03-11, a massive earthquake of magnitude 9.0 occurred in the Tohoku region of Japan. The resulting gigantic tsunami caused catastrophic damage to Fukushima Daiichi Nuclear Power Plant (Chino et al., 2011) and the discharge of an enormous quantity of nuclear waste into the nearby ocean and land. The contamination by cesium isotopes, such as Cs^{134} ($T_{1/2} = 2$ years) and Cs^{137} ($T_{1/2} = 30.2$ years), was one of the major environmental concerns. Once radioactive cesium enters the environment through soil, river water, and seawater, it can incorporate easily into the human body through the food chain (Arai, 2014; Doi et al., 2012). Radioactive cesium accumulates primarily in muscle and bone and causes cancer (Fisher et al., 2013). Various excellent remediation techniques have been developed to date for eliminating radioactive materials and toxic metals (Wang et al., 2019; Xie et al., 2019a,b, Xie et al., 2019a,b). Given its toxicity, economic and safe removal techniques for radioactive cesium are needed.

Prussian blue (PB) is a versatile adsorbent for the selective elimination of radioactive cesium. PB has unique crystal structure and thereby is capable of hosting small molecules (water) and ions (K^+ , Na^+ , NH_4^+ or Cs^+) in their crystal lattice spaces. PB selectively adsorb cesium because of its promising size-recognition of hydrated Cs^+ (Ishizaki et al., 2013). Generally, there are just two types of PB: one type is insoluble with a chemical formula of $\text{Fe}_4^{\text{III}}[\text{Fe}^{\text{II}}(\text{CN})_6] \cdot x\text{H}_2\text{O}$ ($x = 14\text{--}16$), and the other type is soluble in water with a chemical formula of $\text{KFe}^{\text{III}}[\text{Fe}^{\text{II}}(\text{CN})_6]$. (Buser et al., 1977; Pearce, 1994). Moreover, PB has several analogs that have superior performance compared to ordinary PB (Takahashi et al., 2015, 2016; Takahashi et al., 2018). Researchers have studied PB-based adsorbent materials, such as graphene/PB composite (Yang et al., 2014), beads (Vipin et al., 2013, 2014; Parajuli et al., 2016), spongiforms (Yu et al., 2010; Hu et al., 2012; Vipin et al., 2016), fabrics (Chen et al., 2015), and yarns (Okamura et al., 2014), that have demonstrated excellent performance and technique for the adsorption of cesium ions. However, the major weak point of PB is its instability in alkaline solutions, which causes hazardous cyanide contamination (Faustino et al., 2008; Ware, 2009). It is practically impossible to neutralize a cesium-contaminated solution, especially a large volume of seawater (pH 8.1). Therefore, the stabilization of PB is highly necessary before it can be used in an alkaline solution and seawater.

WHO has established guidelines for total cyanide (TCN) concentration in drinking water, with a regulatory upper limit of 0.07 mg/L. In Japan, TCN regulations require a detection limit less than 0.01 mg/L for water quality standards and 0.1 mg/L for environmental standards (G of J. Ministry of Environmental, 2015). The drainage standard based on these regulations for the maintenance of the Fukushima living environment is less than 0.5 mg/L (Drainage standard, 2018).

In previous research, a PB precipitate named PB-X [X: bivalent metal] was used to remove cesium ions from a fly ash washing solution and seawater (Ubara et al., 2014, 2018). PB-X demonstrated high cesium removal and efficiency, and the resulting TCN in the solution was below Fukushima limitations. The major drawback of this method was its highly complicated preparation process. The method was suitable only in a narrow pH range near neutral; thus, pH adjustment was essential. Additionally, the separation of adsorbent after decontamination required polymer flocculants.

In our previous research, we developed cellulose nanofiber (CNF)-backboned PB (CNF/PB) that homogeneously fills in a polyurethane sponge (PUF) (Vipin et al., 2016). In the present research, we mainly focus on the structural stabilization of PB and its applicability in alkaline solutions. We demonstrate that stabilization can be achieved by adding CuSO_4 to PB, so that the divalent copper ions act as a shielding element at a high concentration of hydroxide ions. Divalent transition metal ions such as Mn^{2+} , Fe^{2+} , Co^{2+} , Ni^{2+} , Cu^{2+} , and Zn^{2+} could be possible as stabilizer for PB structure. According to the Ubara et al.,

2014, the leaking of copper ions from the PB-Me(OH)₂ (Me; transition metal) was less compared to other transition metal ions with PB. In this research, we selected copper because of its less toxicity, higher oxidation stability, and low-cost compared to other transition metals. Additionally, CNF/PB/ CuSO_4 succeeded in suppressing the leaking of extremely dangerous cyanide from PB, so that the adsorbent is chemically stable and safe in adverse conditions. We conducted complete confirmation experiments on the stability and safety of PB/ CuSO_4 in various alkaline solutions and comprehensively explained the reaction mechanism. To the best of our knowledge, this is the first report that explains the mechanism of PB stabilization using CuSO_4 at high pH in exquisite detail.

2. Materials and methods

2.1. Materials

Prussian blue analog $\text{NH}_4\text{Fe}^{\text{III}}[\text{Fe}^{\text{II}}(\text{CN})_6]$ ($\text{NH}_4\text{-PB}$; commercial trade name is MILOLI BLUE) was purchased from Dainichiseika Color & Chemicals Mfg., Ltd. TEMPO cellulose nanofiber gel (solid fraction: 2 wt %) was purchased from DKS Co. Ltd. $\text{CuSO}_4 \cdot 5\text{H}_2\text{O}$ was purchased from Wako Chemical, Japan.

Isocyanate prepolymer, a mixture of prepolymer (75 %–85 %) and tolylene diisocyanate isomer (15 %–25 %), was purchased from Toyo Quality One Corporation. Pluronic L-62, a tri-block type of copolymer used to strengthen the surfaces of the polyurethane foam, was purchased from ADEKA Corporation.

Natural and artificial seawater (Supporting information Table S1) was purchased from NAZEME 10, Japan QCE Blue Lab Co. Ltd. and MARINE ART SF-1, Osakayakken Co. Ltd., respectively. The reagent and instrument sets to measure total cyanide (TCN) concentration were purchased from Kyoritsu Chemical-Check Lab. Corp.

2.2. Preparation of CNF/ $\text{NH}_4\text{-PB}$ / CuSO_4 composite

A complex of 1000 g of 2 wt% CNF and 160 g of $\text{NH}_4\text{-PB}$ were mixed in a ball mill for three days. Then, 120 ml of 1 M $\text{CuSO}_4 \cdot 5\text{H}_2\text{O}$ was added to the CNF/ $\text{NH}_4\text{-PB}$ complex, and the mixing was continued in same ball mill. After three hours of mixing, we obtained a homogenous composite of CNF/ $\text{NH}_4\text{-PB}$ / CuSO_4 in which the molar ratio of CuSO_4 / $\text{NH}_4\text{-PB}$ was 0.36. We dried the composite at various ratios in the oven for use in the TCN experiments.

2.3. Preparation of spongiform adsorbent encapsulated with CNF/ $\text{NH}_4\text{-PB}$ / CuSO_4

CNF/ $\text{NH}_4\text{-PB}$ / CuSO_4 composite gel was poured into the polyurethane prepolymer along with Pluronic L-62 and mixed vigorously for 1 min. The weight ratio of CNF/ $\text{NH}_4\text{-PB}$ / CuSO_4 composite/polyurethane/Pluronic-L-62 was 46/40/0.4. The adsorbent was dried at 70 °C for 24 h and washed well with deionized water. In this paper, we denote the adsorbent as CNF/ $\text{NH}_4\text{-PB}$ / CuSO_4 /PUF.

2.4. Characterization of materials

The morphology of the samples was observed using a JEOL JSM 6390 scanning electron microscope (SEM). FT-IR spectra were acquired with a JASCO FT/IR-460. X-ray diffraction (XRD) measurements were conducted with a Rigaku SmartLab Multipurpose diffractometer using a Cu - $\text{K}\alpha$ ray at 40 kV and 45 mA. Multifunctional scanning X-ray photoelectron spectrometry (XPS) was conducted with a PHI5000 VersaProbe (Ulvac PHI), and spectral analysis used MultiPAK version 9.0 software. Both the XRD and XPS measurements were performed in the Advanced Characterization Nanotechnology Platform at the University of Tokyo.

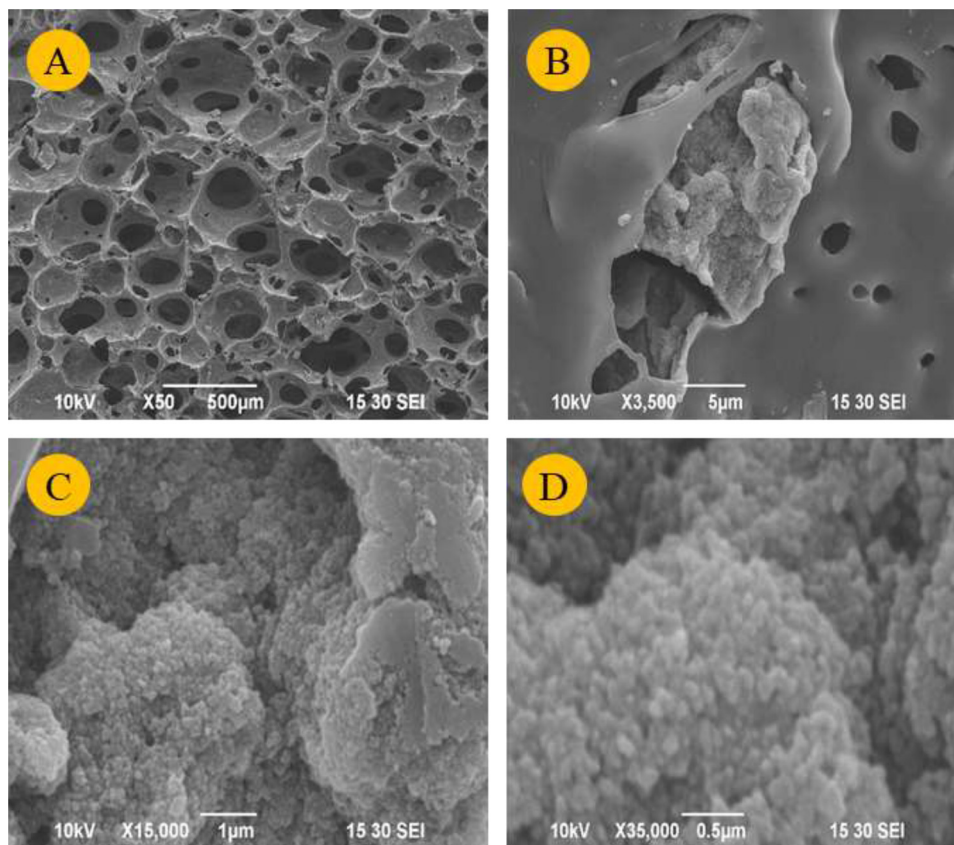


Fig. 1. SEM image of CNF/NH₄-PB/CuSO₄/PUF. (A) Magnification at 50 × . (B) Magnification at 3500 × . (C) Magnification at 15,000 × . (D) Magnification at 35,000 × .

2.5. Adsorption capacity and rate analysis

We conducted a batch experiment to understand the adsorption capacity, using an initial cesium concentration that ranged from 10 ng/L to 10 mg/L. First, 200 mg of adsorbent was put in 40 ml of cesium solution with the desired initial concentration, and it was shaken for five hours in a vortex shaker at 600 rpm and 25 °C. The cesium concentration in the batch experiments was measured using inductively coupled plasma mass spectrometry (ICP-MS, Parkin Elmer Elan DRC-e) and atomic absorption spectrometry (AAS, HITACHI Z-2000). AAS was especially used to measure the high levels of cesium concentration in seawater.

The determination of the adsorption capacity for cesium used the following:

$$q = \frac{V(C_0 - C_e)}{m} \quad (1)$$

where C_0 and C_e are the initial and final concentrations (mg/L) of absorbable ions, V is the volume (L) of the aqueous solution, and m is the weight (g) of the adsorbent.

Similarly, we conducted a batch test with initial Cs concentrations from 100 ng/L to 1000 ng/L to understand the mechanism and rate of adsorption. The adsorption of cesium follows the pseudo-second-order rate law

$$\frac{t}{q_t} = \frac{1}{k_2 q_i^2} + \frac{t}{q_i} \quad (2)$$

where k_2 is the pseudo-second-order rate constant, q_t (Cs-ng/g-adsorbent) is the amount of cesium adsorbed at time t (min), and q_i (Cs-ng/g-adsorbent) is the amount adsorbed at equilibrium.

To understand the detailed adsorption behavior and mechanism, isotherm equations were applied. In this study, we used the Langmuir

(Eq. (3)) and Freundlich (Eq. (4)) isotherm models:

$$q_e = \frac{q_m K C_e}{1 + K C_e} \quad (3)$$

where q_e is the absorption capacity (mg/g) at equilibrium; C_e is the equilibrium concentration (mg/L); and q_m and K are Langmuir constants related to maximum adsorption capacity (mg/g) and energy of adsorption (L/mg), respectively; and

$$\ln q_e = \ln K_f + \frac{1}{n_f} \ln C_e \quad (4)$$

where q_e is the equilibrium solid phase concentration (mg/g); K_f and n_f are the isotherm parameters of adsorption capacity (mg/g) and adsorption intensity, respectively; and C_e is the equilibrium liquid phase concentration (mg/L).

2.6. Evaluation of cyanide suppression from NH₄-PB/CuSO₄ composite powders and the adsorbent

The TCN concentration from the samples was measured by following Japanese standard method JIS standard (JIS K 0400-38-102., 1999). This method, conducted with distillation and picric acid absorptiometry, used the instrument Lambda-9000, DIGITALPACKT-EST-MULTI. For the evaluation of TCN concentration from NH₄-PB/CuSO₄ powders, 0.1 g each of various composites were shaken at 600 rpm under 30 °C in 100 ml of natural seawater for three days. Similarly, we experimented with artificial river water at various pH values, from 1 to 13 (pH adjusted using Ca(OH)₂ and H₂SO₄), at 30 °C. Moreover, the relationship between temperature and cyanide leaking was analyzed by conducting a batch study in artificial seawater and natural seawater at temperatures ranging from 10 °C–50 °C for four days.

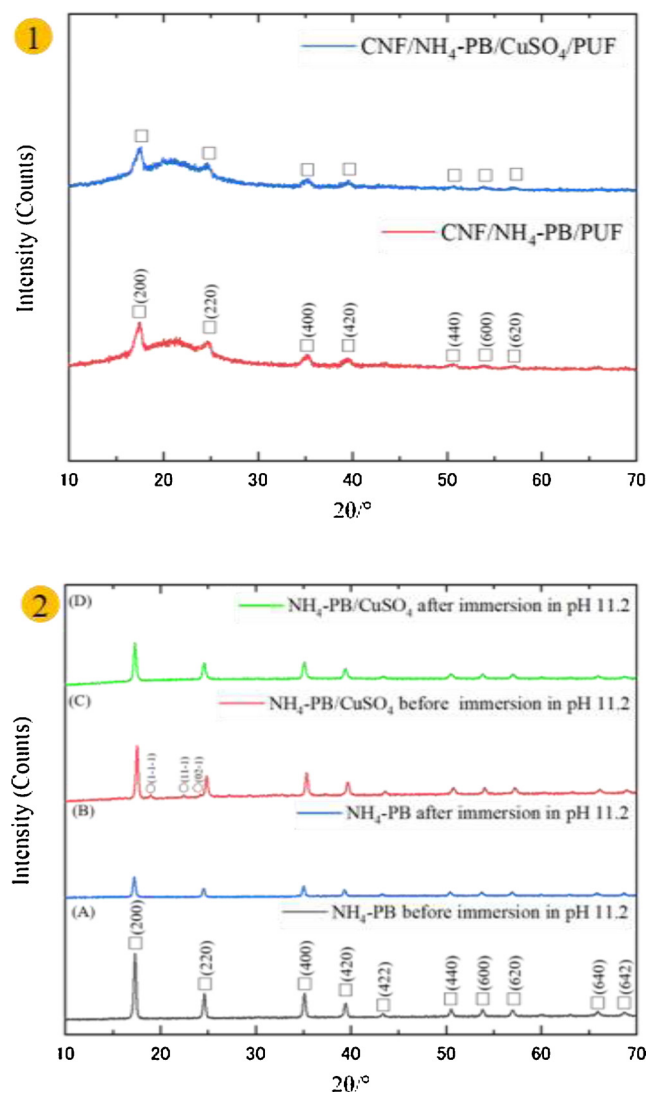


Fig. 2. (1) XRD patterns of CNF/NH₄-PB/PUF and CNF/NH₄-PB/CuSO₄/PUF. (2) XRD patterns for (A) NH₄-PB before and (B) after immersion in a solution at pH 11.2. (C) NH₄-PB/CuSO₄ (at molar ratio 0.36) before and (D) after immersion in a solution at pH 11.2.

3. Results and discussion

The porous structure and surfaces of the CNF/NH₄-PB/CuSO₄/PUF are clearly visible in the low-magnification SEM image in Fig. 1(A). Fig. 1(B) shows the encapsulation of CNF/NH₄-PB/CuSO₄ in the surfaces of the PUF. Furthermore, Fig. 1(C) and (D) show that CNF/NH₄-PB/CuSO₄ nanoparticles with an average size of 100 nm were clustered together and densely packed inside the PUF surfaces.

The XRD patterns of CNF/NH₄-PB/PUF and CNF/NH₄-PB/CuSO₄/PUF are shown in Fig. 2(1). The XRD of NH₄-PB (Fig. 2(2)) showed characteristic diffraction peaks as Fm-3m at 17.3°, 24.6°, 35.1°, 39.4°, 43.3°, 50.5°, 53.8°, 57.0°, 65.9°, and 68.7°, which correspond to the (200), (220), (400), (420), (422), (440), (600), (620), (640), and (642) planes (DB card number 00-061-1256) (Ishizaki et al., 2013), respectively. These peaks can be mainly seen in the CNF/NH₄-PB/PUF and CNF/NH₄-PB/CuSO₄/PUF patterns in Fig. 2(1). The XRD patterns in Fig. 2(2)(A) and (B) show the original NH₄-PB before and after immersion in solution at a pH level of 11.2; similarly (C) and (D) show NH₄-PB/CuSO₄ (molar ratio 0.36) before and after immersion in a solution at pH 11.2.

Fig. 2(2) shows XRD patterns of NH₄-PB and NH₄-PB/CuSO₄ before

and after immersion in a solution with pH 11.2. The composite was immersed in a high pH solution overnight, then the collected samples were freeze-dried without washing and the XRD pattern was obtained. NH₄-PB/CuSO₄ had the same peaks as NH₄-PB (Fig. 2(2)(A)). Additional CuSO₄ peaks (DB card number 01-072-2356) were also found in the NH₄-PB/CuSO₄ pattern at 18.95°, 22.48°, and 24.16°, which correspond to the (1-1-1), (11-1), and (02-1) planes, respectively. Also, the peaks of CuSO₄ overlap with those of NH₄-PB from 40° to 60°. The XRD patterns of NH₄-PB and NH₄-PB/CuSO₄ after immersion in the solution at pH 11.2 were similar to those of the original NH₄-PB. The XRD of NH₄-PB after immersion in a high pH solution confirmed that a significant portion of the crystals decomposed in the absence of CuSO₄. However, the intensity of NH₄-PB/CuSO₄ before and after immersion in a high pH solution remain unchanged, indicating that the entire crystals were protected. Thus, it was confirmed that copper sulfate was a protecting element for PB crystals.

XPS spectra of CNF/NH₄-PB and CNF/NH₄-PB/CuSO₄ are shown in Fig. 3(A). The wide XPS spectrum of CNF/NH₄-PB showed the elemental peaks of C, N, O, and Fe derived from NH₄-PB, as well as the Na peaks derived from TEMPO CNF. The elemental peaks of Cu and S were clearly visible in the wide spectrum of CNF/NH₄-PB/CuSO₄ (molar ratio 0.36).

Fig. 3(B) shows the XPS spectra for NH₄-PB before and after immersion in a solution at pH 11.2 as well as for NH₄-PB/CuSO₄ composite before and after immersion. The characteristic peak Cu2p of CuSO₄ was detected in the NH₄-PB/CuSO₄ composite before and after immersion in the solution. However, characteristic peaks such as S2s and S2p from CuSO₄ were not detected in NH₄-PB/CuSO₄ after immersion in a solution with pH 11.2, which confirmed the chemical reaction of the copper ions. Fig. 3(C) and (D) show the XPS narrow spectra at O1s of NH₄-PB/CuSO₄ composite before and after immersion at pH 11.2. These results confirm that mainly two peaks at O1s appeared after immersion compared to before immersion and that CuSO₄ converted to Cu(OH)₂ and CuO after immersion (Cano et al., 2001; Hsu et al., 2012; Cheng et al., 2013). Fig. 3(E) shows the XPS spectra at S2p of the NH₄-PB/CuSO₄ composite. The intensity of the S2p peak after immersion was reduced compared to before immersion. From these results, it was assumed that the SO₄²⁻ of CuSO₄ reacted with H⁺ or Na⁺ ions in the solution with high pH, and that Cu of CuSO₄ was converted into Cu oxides, such as Cu(OH)₂ and CuO, which contributed to a reduction in pH.

Fig. 4(A) shows the adsorption rate using CNF/NH₄-PB/CuSO₄/PUF at two initial cesium concentrations: 100 and 1000 ng/L. Fig. 4(B) provides a linear fit to the pseudo-second-order kinetic equation. According to these linear equations, the values of the correlation efficiency R² at 100 and 1000 ng/L were 0.99994 and 0.99989, respectively. Thus, both R² were well fitted the pseudo-second-order kinetic adsorption rate. In addition, the nonlinear fitting (Fig. S1) also confirmed that the adsorption fits well with the pseudo-second-order kinetic rate. K₂ is 0.016 (Cs: 100 ng/L) and 0.0013 (Cs: 1000 ng/L), and the initial adsorption rate constant V₀ (ng / g-min) is 5.85 (Cs: 100 ng/L) and 44.44 (Cs: 1000 ng/L). The adsorption in the ppm (mg/L) order of the Cs concentration was also well fitted with a pseudo-second-order kinetic equation, as shown in Fig. S2. The R² value of the pseudo-second-order kinetic equation was 0.9999. From these results, we understood that the adsorption was well fitted by the pseudo-second-order kinetic model in Cs solutions with concentrations that ranged from ppt (ng/L) to ppm (mg/L).

The adsorption occurred with CNF/NH₄-PB/CuSO₄/PUF at low and high cesium concentrations. The fitting of the experimental data with the Langmuir and Freundlich adsorption isotherm models is shown in Fig. 4(C). At the low concentration, Fig. 4(C) indicates that the experimental data better fit the Freundlich adsorption isotherm than the Langmuir model. The reason was because the adsorbent adsorbed more than 99 % of the cesium ions at extremely low concentrations. However, the adsorption with a high concentration of cesium ions from

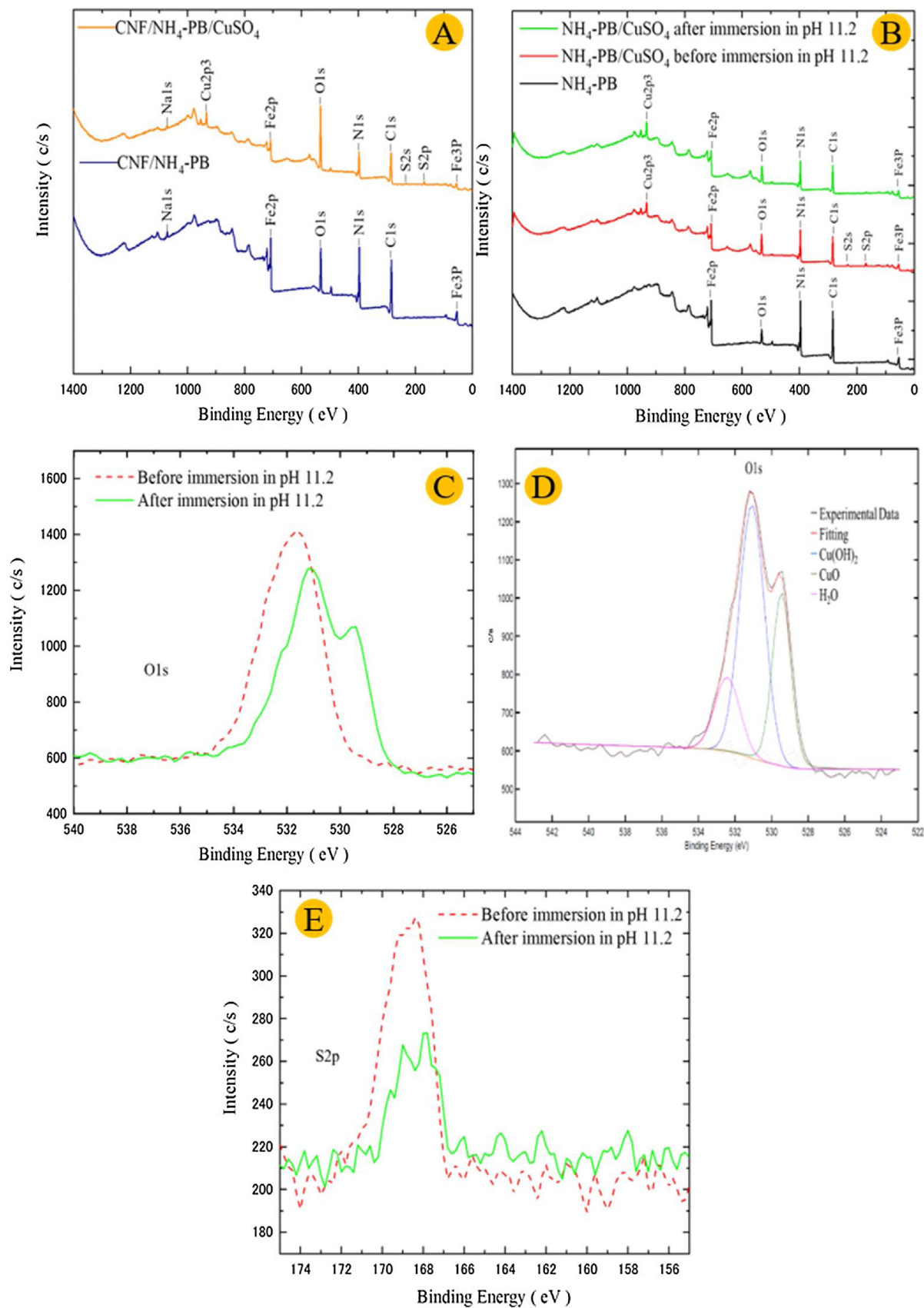


Fig. 3. (A) Wide-scan XPS spectra of CNF/NH₄-PB and CNF/NH₄-PB/CuSO₄. (B) Wide-scan XPS spectra of NH₄-PB and NH₄-PB/CuSO₄ (molar ratio 0.36). (C) and (D) O1s spectra of NH₄-PB/CuSO₄ and curve fitting after immersion in a high pH solution, respectively. (E) S2p spectra of NH₄-PB/CuSO₄.

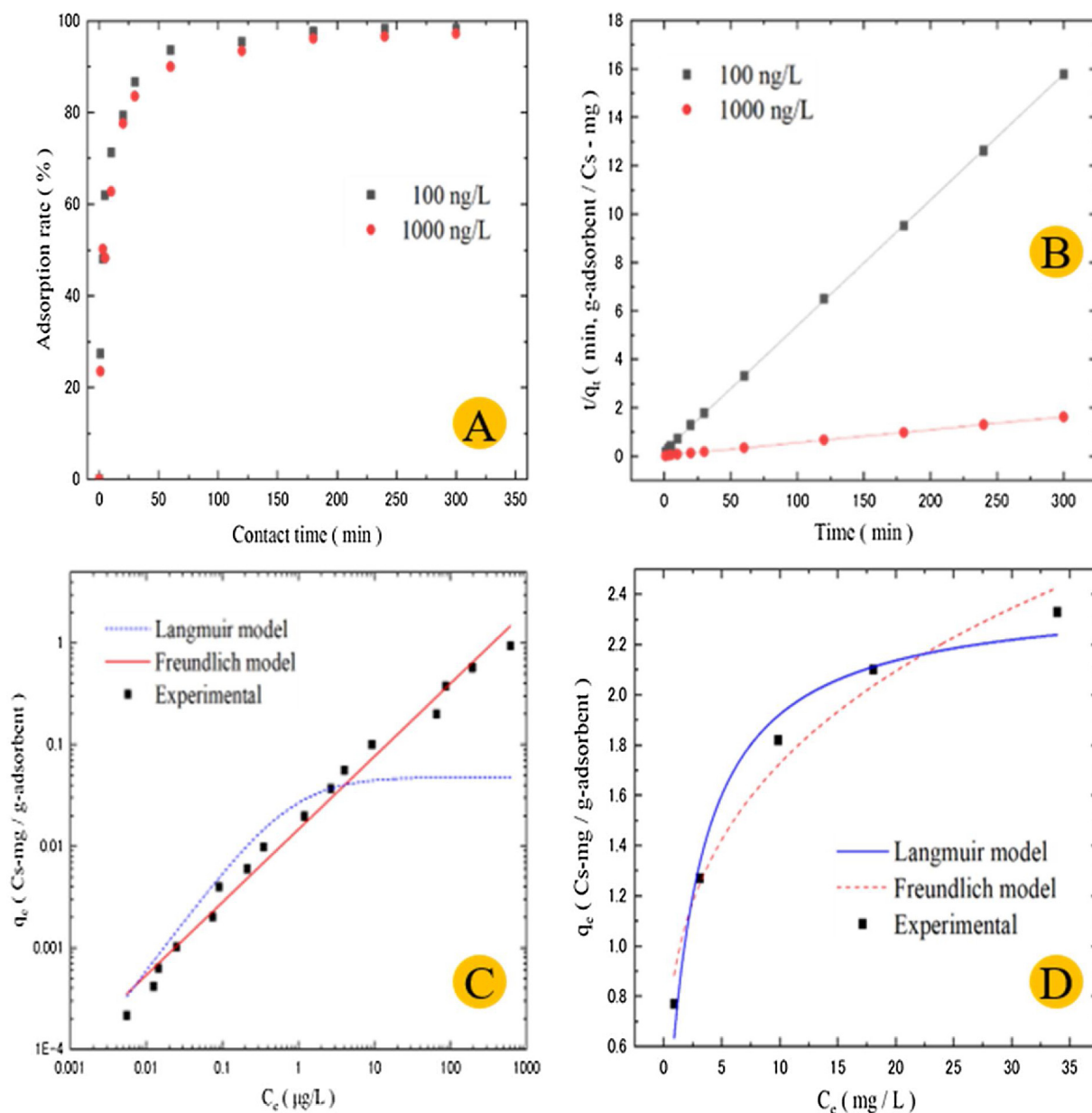


Fig. 4. (A) Adsorption rate (%). (B) Pseudo-second-order plots using CNF/NH₄-PB/CuSO₄/PUF in deionized water. (C) and (D) The Langmuir and Freundlich adsorption isotherm fitting at low (deionized water) and high (seawater) cesium concentrations, respectively.

seawater followed the Langmuir model better than the Freundlich adsorption isotherm (Fig. 4(D)).

In this study, the adsorbent (CNF/NH₄-PB/CuSO₄/PUF) includes CNF, which can bind with metal ions. Therefore, CNF helps to prevent the leaking of copper sulfate from the adsorbent. Thus, the utilization of copper sulfate has no problem in the environment. We measured the copper leaking from CNF/NH₄-PB/CuSO₄/PUF during cesium decontamination (Supporting information Fig. S3). The copper ions presented in the neutral solution while using CNF/NH₄-PB/CuSO₄/PUF at molar ratio 0.36 was 3.3 mg/L. Since the PB is highly stable at neutral pH, stabilization using copper sulfate is not necessary. However, the maximum value of copper ions in the case of initial pH 11.2 was only 0.22 mg/L. The value is below the drainage regulatory upper limit of 2 mg/L (Fukushima drainage standard., 2018), indicating that there was no secondary copper pollution from the adsorbent. So, the new stabilized adsorbent was highly safe for the application of cesium decontamination from alkaline solutions.

A comparison of the Cs adsorption capacity between deionized

water and seawater is shown in the supporting information, Fig. S4. From these results, the maximum adsorption capacity was Cs-2.45 mg/g-adsorbent and remained unchanged in both deionized water and natural seawater. The results confirmed that PB could use both neutral and alkaline solutions for the selective decontamination of cesium. We compared the adsorption capacity of both CNF/NH₄-PB/CuSO₄/PUF and CNF/NH₄-PB/PUF and the results shown in the supporting information Fig. S5. The adsorption capacity of both adsorbents were the same value. The results confirmed that the stabilization using copper sulfate not affect the cesium adsorption capacity of the original PB.

Fig. 5(A) shows the concentration of TCN in artificial river water at various pH values while using CNF/NH₄-PB/CuSO₄/PUF. The initial pH value was adjusted between 1 and 13. The results confirmed that the TCN concentration was less than 0.5 mg/L at all pH values except 12 and 13. In particular, the TCN concentration was less than 0.04 mg/L from pH 3–11. In the case of pH 1, the TCN concentration had a comparably higher value, 0.13 mg/L. In summary, we confirmed that CNF/NH₄-PB/CuSO₄/PUF was highly stable, and the cyanide

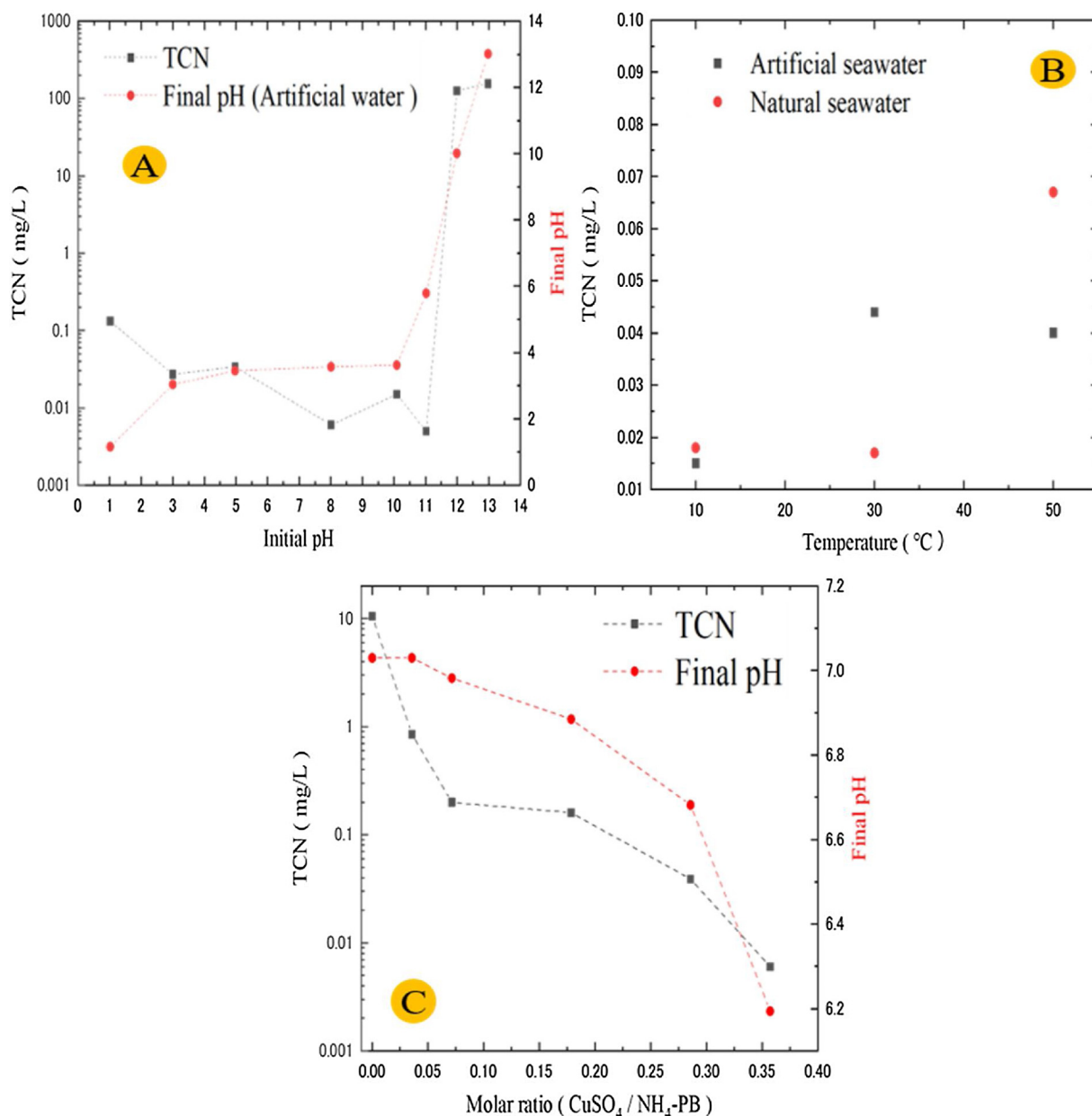


Fig. 5. (A) TCN concentration and initial/final pH value in artificial river water after immersion of CNF/NH₄-PB/CuSO₄/PUF. (B) TCN concentration from CNF/NH₄-PB/CuSO₄/PUF in artificial and natural seawater. (C) Variation in TCN concentration and final pH values depending on the molar ratio between NH₄-PB and CuSO₄.

concentration in the solution was under the permissible level when the pH was in the range 1–11. The TCN concentration at pH 12 and 13 was more than 120 mg/L, which assumed that the state of the NH₄-PB structure was unstable and gradually broken. From pH 1–3, the final pH value was almost the same as the initial value. However, from pH 5–11, the final pH was considerably lower than the initial value. Moreover, this confirmed that the final pH dropped below the neutral value. In the case of pH 12 and 13, the former pH was reduced to 10, and the latter was almost the same as the initial value.

Fig. 5(B) compares the TCN concentrations from CNF/NH₄-PB/CuSO₄/PUF in artificial seawater and natural seawater at temperatures between 10 °C–50 °C. The results confirmed that the TCN concentrations in the solution at all temperature conditions were under the environmental regulatory value. Fig. 5(C) showed variations in the TCN and final pH depending on the molar ratio of NH₄-PB and CuSO₄ in natural seawater at pH 8.1. When the molar ratio was 0.05 or more, the TCN concentrations were 0.2 mg/L or less, and when the molar ratio

was 0.05 or less, the TCN concentrations were 0.8 mg/L or more. In contrast, the TCN concentration had an extremely high value of 10.5 mg/L in the case of NH₄-PB without CuSO₄.

Fig. 5(C) confirmed that the TCN concentration was decreased by increasing CuSO₄, and, finally, the TCN concentration was reduced to 0.006 mg/L at the molar ratio of 0.36. On the other hand, the final pH value when using only NH₄-PB was 7.0 and was gradually reduced by adding more CuSO₄. Finally, the final pH value of seawater when using NH₄-PB/CuSO₄ at a molar ratio of 0.36 was 6.2.

The stability of PB at high pH depending on the molar ratio between NH₄-PB and CuSO₄. We tested with a higher volume of seawater where the liquid/solid ratio was 10,000. The data shown in the supporting information Table S2. The final pH of the seawater was 7.36; however, TCN in the solution remained under the regulatory value. A comparison of final seawater color after immersion of NH₄-PB and NH₄-PB/CuSO₄ shown in supporting information Fig. S6. The decomposed NH₄-PB gave a brownish color to the seawater. The seawater color was unchanged

Table 1

Comparison of pH values and total cyanide concentrations between NH₄-PB and NH₄-PB/CuSO₄. The composite and solution volumes were 0.1 g and 100 ml, respectively.

Sample name	pH		Total cyanide mg/L
	Initial	Final	
NH ₄ -PB	11.2	6.4	45.0
NH ₄ -PB/CuSO ₄ (molar ratio at 0.36)	11.2	5.4	0.006

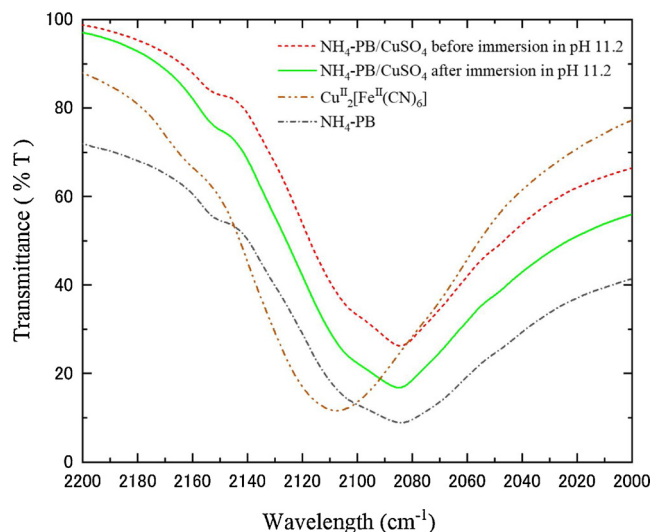
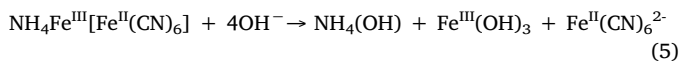


Fig. 6. FT-IR spectra representing NH₄-PB, NH₄-PB/CuSO₄ (molar ratio 0.36) before and after immersion in a solution at pH 11.2, and Cu₂[Fe^{II}(CN)₆].

after immersion of NH₄-PB/CuSO₄, confirmed the stability.

Table 1 shows the pH changes and TCN in the solution from NH₄-PB and NH₄-PB/CuSO₄. The initial pH value in both cases was set at 11.2, which was adjusted using NaOH. After immersing the powdered NH₄-PB in the solution, the final pH value was decreased to 6.4 and that of NH₄-PB/CuSO₄ was 5.4. On the other hand, the TCN value in the NH₄-PB was extremely high, and it was reduced tremendously by incorporated CuSO₄, as given in **Table 1**. From the results, we confirmed that NH₄-PB, after being immersed in a solution without CuSO₄ at pH 11.2, was decomposed. We assumed that Fe in the NH₄-PB turned into Fe(OH)₃; (Eq. (5)) therefore, the pH value changed from alkali to neutral.



A higher amount of chelated cyanide ions were released into the solution in the absence of a central metal ion. However, in the case of NH₄-PB/CuSO₄, the copper ion prevents the hydroxide ion from attacking the iron of PB.

Supporting information Table S3 compared the TCN concentrations for artificial river water at pH 9.1 and natural seawater at pH 8.1. The TCN concentrations from both NH₄-PB/CuSO₄ and CNF/NH₄-PB/CuSO₄ powder, with the molar ratio of CuSO₄/NH₄-PB equal to 0.36, were under 0.1 mg/L. These results revealed that the presence of copper sulfate contributed to the suppression of the leaking of cyanide complexes from the PB. We compared the alkaline stability of NH₄-PB and Cu₂[Fe^{II}(CN)₆]. The TCN concentration of NH₄-PB was about 3 times higher than that of Cu₂[Fe^{II}(CN)₆] in both conditions. This revealed that NH₄-PB decomposed more than Cu₂[Fe^{II}(CN)₆].

Fig. 6 shows the FT-IR spectra of NH₄-PB, NH₄-PB/CuSO₄ before and after immersion at pH 11.2, and Cu₂[Fe^{II}(CN)₆]. The FT-IR peak at

2072 cm⁻¹ is known as the C≡N stretching vibration. The C≡N stretching vibration peak of NH₄-PB and NH₄-PB/CuSO₄ before and after immersion at pH 11.2 was confirmed at 2085 cm⁻¹, and the peak of Cu₂[Fe^{II}(CN)₆] was at 2107 cm⁻¹. From this result, we understood that NH₄-PB after immersion at pH 11.2 was not involved in the chemical reaction within the Cu²⁺. Thus, Fe of NH₄-PB did not occur as a replacement within copper ions in the CuSO₄.

The XRD pattern in **Fig. 2(2)** and **Table 1** confirm the crystalline and chemical states of PB protected by copper sulfate. The FTIR data in **Fig. 6** proved that there was no divalent iron, and copper ionic replacement occurred. The decrease in initial pH value (**Table 1**) confirmed the chemical reaction. The chemical changes in copper sulfate at high pH were confirmed by the XPS narrow spectra of O1s in **Fig. 3(D)**. In summary, the CuSO₄ covered the NH₄-PB crystal and reacted with OH⁻ ions at high pH. This protected the NH₄-PB from decomposition.

4. Conclusion

In this research, we demonstrated the utilization of copper sulfate as a stabilizer for PB and developed a composite spongiform adsorbent. We combined a complex of ammonia PB and CNF with copper sulfate solution and then made a spongiform adsorbent using PUF. The stability of the adsorbent was confirmed under various pH (1–11.2) and temperature (10 °C–50 °C) conditions. The TCN that escaped from stabilized PB at pH 11.2 was only 0.006 mg/L, and that of PB was 45 mg/L. Furthermore, the stabilization kept the crystalline structure unchanged, even after immersion at pH 11.2. The reaction mechanism confirmed by XRD, FTIR, and XPS analysis revealed that, at high pH, copper ions reacted with hydroxide ions and protected the inner PB crystals. More importantly, the new stabilized PB showed promising cesium adsorption that would be suitable under extreme environmental conditions.

Authors contribution

The research idea was proposed by S.M., A.K.V., and B.F. The experiments were designed and performed by S.M., A.K.V., T.K., S.T., and B.F. The composite and spongiform was made by S.M. The data was analyzed and discussed the interpretation of results by S.M., A.K.V., B.F., and I. S. The manuscript; the revision and editing of the manuscript was performed by S.M., A.K.V., B.F., and I. S.

Declaration of Competing Interests

We have no conflicts of interest to disclose.

Acknowledgment

T.K and S.T. acknowledge the support from Nanosummit Co. Ltd, Japan.

Appendix A. Supplementary data

Supplementary material related to this article can be found, in the online version, at doi:<https://doi.org/10.1016/j.jhazmat.2019.121979>.

References

- Arai, T., 2014. Radioactive cesium accumulation in freshwater fishes after the Fukushima nuclear accident. Springerplus 3, 13.
- Buser, H.J., Ludi, A., Schwarzenbach, D., Petter, W., 1977. The crystal structure of prussian blue: Fe₄[Fe(CN)₆]₃·xH₂O. Inorg. Chem. 16, 2704–2710.
- Cano, E., Torres, C.L., Bastidas, J.M., 2001. An XPS study of copper corrosion originated by formic acid vapour at 40% and 80% relative humidity. Mater. Corros. 52, 667–676.
- Chen, G.R., et al., 2015. Prussian blue non-woven filter for cesium removal from drinking water. Sep. Purif. Technol. 153, 37–42.
- Cheng, Z., Du, M., Lai, H., Zhang, N., Sun, K., 2013. From petal effect to lotus effect: a facile solution immersion process for the fabrication of super-hydrophobic surfaces

- with controlled adhesion. *Nanoscale* 5, 2776–2783.
- CHINO, M., et al., 2011. Preliminary estimation of release amounts of ¹³¹I and ¹³⁷Cs accidentally discharged from the Fukushima Daiichi nuclear power plant into the atmosphere. *J. Nucl. Sci. Technol.* 48, 1129–1134.
- Doi, H., Takahara, T., Tanaka, K., 2012. Trophic position and metabolic rate predict the long-term decay process of radioactive cesium in fish: a meta-analysis. *PLoS One* 7, 1–6.
- Drainage standard based on the regulations about maintenance of Fukushima living environment (2018). <https://www.pref.fukushima.lg.jp/uploaded/attachment/167603.pdf>.
- Faustino, P.J., et al., 2008. Quantitative determination of cesium binding to ferric hexacyanoferrate: Prussian blue. *J. Pharm. Biomed. Anal.* 47, 114–125.
- Fisher, N.S., et al., 2013. Evaluation of radiation doses and associated risk from the Fukushima nuclear accident to marine biota and human consumers of seafood. *Proc. Natl. Acad. Sci.* 110, 10670–10675.
- G. of J. Ministry of Environment, 2015. Setting the Basic Environmental Standards (in Japanese). (Accessed January 25, 2015). <http://www.env.go.jp/council/09water/y095-05/mat05.pdf>.
- Hsu, Y.K., Chen, Y.C., Lin, Y.G., 2012. Characteristics and electrochemical performances of lotus-like CuO/Cu(OH)₂ hybrid material electrodes. *J. Electroanal. Chem.* 673, 43–47.
- Hu, B., Fugetsu, B., Yu, H., Abe, Y., 2012. Prussian blue caged in spongiform adsorbents using diatomite and carbon nanotubes for elimination of cesium. *J. Hazard. Mater.* 217–218, 85–91.
- Ishizaki, M., et al., 2013. Proton-exchange mechanism of specific Cs⁺ adsorption via lattice defect sites of Prussian blue filled with coordination and crystallization water molecules. *Dalton Trans.* 42, 16049–16055.
- JIS K 0400–38-10, 1999. Japanese Industrial Standard Committee: Water Quality – Determination of Cyanide, Part 1 – Determination of Total Cyanide. Japan.
- Okamura, Y., et al., 2014. Cesium removal in freshwater using potassium cobalt hexacyanoferrate-impregnated fibers. *Radiat. Phys. Chem.* 94, 119–122.
- Parajuli, D., et al., 2016. Comparative study of the factors associated with the application of metal hexacyanoferrates for environmental Cs decontamination. *Chem. Eng. J.* 283, 1322–1328.
- Pearce, J., 1994. Studies of any toxicological effects of Prussian blue compounds in mammals—a review. *Food Chem. Toxicol.* 32, 577–582.
- Takahashi, A., et al., 2015. Simultaneous enhancement of Cs-adsorption and magnetic properties of Prussian blue by thermal partial oxidation. *Bull. Chem. Soc. Jpn.* 88, 69–73.
- Takahashi, A., et al., 2016. Radioactive cesium removal from ash-washing solution with high pH and high K⁺ concentration using potassium zinc hexacyanoferrate. *Chem. Eng. Res. Des.* 109, 513–518.
- Takahashi, A., et al., 2018. Unveiling Cs-adsorption mechanism of Prussian blue analogs: Cs⁺-percolation: via vacancies to complete dehydrated state. *RSC Adv.* 8, 34808–34816.
- Ubara, et al., 2014. Treatment of water contaminated with radiocesium using novel complexes between Prussian-blue and bivalent transition metal hydroxides. *Trans. At. Energy Soc. Jpn.* 13, 127–135.
- Ubara, et al., 2018. Chemical structure, formation mechanism, and Cs ion adsorption mechanism of a novel prussian blue (PB) complex (discussion based on HSAB principle). *Kinzoku* 88, 36–43.
- Vipin, A.K., Hu, B., Fugetsu, B., 2013. Prussian blue caged in alginate / calcium beads as adsorbents for removal of cesium ions from contaminated water. *J. Hazard. Mater.* 258–259, 93–101.
- Vipin, A.K., Ling, S., Fugetsu, B., 2014. Sodium cobalt hexacyanoferrate encapsulated in alginate vesicle with CNT for both cesium and strontium removal. *Carbohydr. Polym.* 111, 477–484.
- Vipin, A.K., et al., 2016. Cellulose nanofiber backbone Prussian blue nanoparticles as powerful adsorbents for the selective elimination of radioactive cesium. *Sci. Rep.* 6, 1–14.
- Wang, X., et al., 2019. Synthesis of novel nanomaterials and their application in efficient removal of radionuclides. *Sci. China Chem.* 62, 933–967.
- Ware, M., 2009. Prussian blue: artists' pigment and chemists' sponge. *J. Chem. Educ.* 85, 612–620.
- Xie, Y., et al., 2019a. Porous NiFe-oxide nanocubes derived from prussian blue analogue as efficient adsorbents for the removal of toxic metal ions and organic dyes. *J. Hazard. Mater.* 379, 120786.
- Xie, Y., et al., 2019b. Emerging natural and tailored materials for uranium-contaminated water treatment and environmental remediation. *Prog. Mater. Sci.* 103, 180–234.
- Yang, H., et al., 2014. In situ controllable synthesis of magnetic Prussian blue/graphene oxide nanocomposites for removal of radioactive cesium in water. *J. Mater. Chem. A* 2, 326–332.
- Yu, H., Fugetsu, B., 2010. A novel adsorbent obtained by inserting carbon nanotubes into cavities of diatomite and applications for organic dye elimination from contaminated water. *J. Hazard. Mater.* 177, 138–145.